

# Geophysical Research Letters®



## RESEARCH LETTER

10.1029/2025GL115466

E. Lippiello and G. Petrillo contributed equally to this work.

### Key Points:

- A sawtooth-like ground motion pattern during foreshocks may signal an impending large earthquake
- A new index,  $Q$ , detects anomalies in foreshocks, correctly identifying 10 of 11 cases before major earthquakes
- Analyzing earthquake waveforms could help distinguish foreshocks from regular seismic activity, aiding earthquake forecasting

### Supporting Information:

Supporting Information may be found in the online version of this article.

### Correspondence to:

G. Petrillo,  
giuseppe.petrillo@ntu.edu.sg

### Citation:

Lippiello, E., Petrillo, G., Godano, C., & Dal Zilio, L. (2025). Toward recognizing the waveform of foreshocks. *Geophysical Research Letters*, 52, e2025GL115466. <https://doi.org/10.1029/2025GL115466>

Received 19 FEB 2025

Accepted 19 JUN 2025



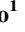

### Author Contributions:

**Conceptualization:** E. Lippiello  
**Data curation:** E. Lippiello, G. Petrillo, C. Godano, L. Dal Zilio  
**Formal analysis:** E. Lippiello, G. Petrillo  
**Funding acquisition:** E. Lippiello, G. Petrillo, L. Dal Zilio  
**Investigation:** E. Lippiello, G. Petrillo  
**Methodology:** E. Lippiello, G. Petrillo  
**Project administration:** E. Lippiello, G. Petrillo, L. Dal Zilio  
**Resources:** E. Lippiello, G. Petrillo  
**Software:** E. Lippiello, G. Petrillo  
**Supervision:** E. Lippiello, C. Godano, L. Dal Zilio  
**Validation:** E. Lippiello, G. Petrillo  
**Visualization:** E. Lippiello, G. Petrillo, C. Godano, L. Dal Zilio

© 2025. The Author(s).

This is an open access article under the terms of the [Creative Commons Attribution License](#), which permits use, distribution and reproduction in any medium, provided the original work is properly cited.

## Toward Recognizing the Waveform of Foreshocks

E. Lippiello<sup>1</sup> , G. Petrillo<sup>2</sup> , C. Godano<sup>1</sup> , and L. Dal Zilio<sup>2,3</sup> 

<sup>1</sup>Department of Mathematics and Physics, University of Campania “L. Vanvitelli”, Caserta, Italy, <sup>2</sup>Earth Observatory of Singapore, Nanyang Technological University, Singapore, Singapore, <sup>3</sup>Asian School of the Environment, Nanyang Technological University, Singapore, Singapore

**Abstract** The identification of seismic precursors remains a fundamental challenge. Foreshocks are often indistinguishable from regular seismic sequences, making it difficult to determine whether they precede a larger rupture. We show that the ground velocity envelope recorded after several  $M_w 6+$  foreshocks exhibits an anomalous sawtooth pattern, distinct from typical post-mainshock signals. This pattern suggests the presence of rate-weakening fault patches approaching instability, promoting stress transfer and aftershock migration into neighboring critically stressed regions. A similar signature was observed in multiple events, including the 2011  $M_w 9.1$  Tohoku earthquake and the 2014  $M_w 8.1$  Iquique sequence. To assess the systematic occurrence of this anomaly, we introduce an index  $Q$  based on the first 45 min of waveform data. Analyzing 68  $M 6+$  earthquakes in selected regions since 2011, we find that 10 of 11 foreshocks preceding a larger event exhibit anomalous  $Q$  values, while only 4 of 57 other events show similar behavior. These findings suggest that foreshock waveform characteristics may provide insight into seismic rupture processes.

**Plain Language Summary** Understanding whether certain earthquakes signal the likelihood of a larger rupture remains a critical question in seismology. In this study, we analyze ground shaking patterns following moderate earthquakes (magnitude 6 and above) to identify anomalous signals that may indicate an impending larger event. We find that some foreshocks exhibit a distinctive sawtooth pattern in their ground motion, which differs from typical earthquake signals. This pattern suggests that parts of the fault may be approaching instability collectively, potentially altering how seismic energy is released. To systematically assess this effect, we introduce a method to quantify these anomalies in the first 45 min of earthquake recordings. Applying this approach to earthquakes from the past 15 years, we find that many foreshocks preceding large earthquakes exhibit this signature. While further research is needed, these findings provide new insights into earthquake sequences and the physical conditions leading to major ruptures.

## 1. Introduction

The existence of precursory signals before large earthquakes remains a central question in seismology (Cicerone et al., 2009; Mignan, 2014; Peng & Lei, 2025; Pritchard et al., 2020; Scholz et al., 1973; Wyss, 1991). Foreshocks, in particular, have been widely investigated as potential precursors, yet their prognostic value is still controversial (Felzer et al., 2004; Petrillo & Lippiello, 2020, 2023; Seif et al., 2019; Zaccagnino et al., 2024). While laboratory experiments and numerical models often reveal accelerating slip prior to failure (Dieterich & Kilgore, 1996; Kaneko et al., 2016; Rubin & Ampuero, 2005), translating these findings to natural faults remains challenging (Hulbert et al., 2019; Passelègue et al., 2017). One key limitation is that laboratory studies typically assume homogeneous fault conditions, whereas natural faults exhibit strong structural and frictional heterogeneity—including localized seismic and aseismic slip, variations in frictional properties, and cascading failure processes—all of which can critically influence rupture nucleation and precursor expression.

Recent advances in seismic and geodetic monitoring have enabled the identification of transient fault activity before some large earthquakes, including slow slip events and foreshock sequences (Beaucé et al., 2023; E. E. Brodsky & Lay, 2014a; A. Kato & Ben-Zion, 2021; Martínez-Garzón & Poli, 2024). Notably, a recent study by Bletery and Nocquet (2023, 2025) suggested the existence of systematic precursory slip in geodetic data, sparking both interest and debate in the scientific community (Bradley & Hubbard, 2023, 2024). However, such transient signals are not systematically observed, and similar activity has often been detected without an ensuing mainshock (Behr & Bürgmann, 2021; Bletery & Nocquet, 2020; Gomberg et al., 2010; Obara & Kato, 2016). This lack of consistency makes it difficult to determine whether seismic sequences exhibit diagnostic signals—observable in seismic or geodetic data—that indicate imminent fault failure.

**Writing – original draft:** E. Lippiello, G. Petrillo, C. Godano, L. Dal Zilio  
**Writing – review & editing:** E. Lippiello, G. Petrillo, C. Godano, L. Dal Zilio

The complexity of fault behavior is often associated with spatial variations in frictional properties, with faults containing regions that either strengthen or weaken as slip rates change (Avouac, 2015). During interseismic periods, rate-strengthening fault patches creep steadily under tectonic loading, while rate-weakening patches remain locked and accumulate stress (N. Kato, 2020; Kazemian et al., 2015; Pelletier, 2000; Lippiello, Petrillo, Landes, & Rosso, 2019; Lippiello et al., 2021; Petrillo et al., 2020). When these locked patches experience stress levels that exceed their local strength, they may undergo seismic slip, perturbing adjacent regions and potentially triggering cascading failure along the fault (McLaskey, 2019; Schwartz & Rokosky, 2007). Large ruptures are generally thought to nucleate within critically stressed fault patches; their growth into major earthquakes depends on the rupture's ability to propagate through heterogeneous fault regions and activate adjacent areas, ultimately leading to collective failure. While rate-and-state friction laws provide a widely used framework for modeling fault slip, they offer only a simplified description of natural rupture processes. Near failure, rupture dynamics are increasingly governed by the structural complexity and topological organization of a fault, which influence how stress is transferred and redistributed across the fault. In this regime, dynamic fracture and long-range interactions can dominate over local frictional properties, suggesting that rupture is better understood as an emergent collective phenomenon rather than the sum of isolated patch instabilities (Fineberg & Marder, 1999; Lee et al., 2024; Reches & Fineberg, 2023). Since direct stress measurements on faults are not feasible, indirect methods are necessary to assess how close a fault is to failure. Geodetic observations provide constraints on slip deficit, but their spatial resolution is often insufficient to resolve fine-scale variations in fault stress (Cohen, 1999; Okada, 1985). Consequently, seismic data remain a critical tool for investigating earthquake nucleation and rupture dynamics.

Seismic waveforms contain rich information about asperities—localized regions where stress accumulates and is released (Lay & Kanamori, 1981; Lei, 2003). Previous studies have shown that the frequency content of seismic waves provides insight into asperity size: smaller asperities radiate higher-frequency waves due to their rapid energy release, whereas larger asperities release energy more slowly, producing lower-frequency signals (Aki, 1967; Kumagai et al., 2012; Sato & Hirasawa, 1973). However, the potential of waveform analysis for identifying evolving fault conditions remains underexplored. In this study, we focus on foreshock waveforms, analyzing 68  $M6+$  earthquakes in selected regions since 2011 that occurred near and shortly before a larger event (Figure 1). Our results show that foreshocks preceding large earthquakes often exhibit characteristic waveform patterns—marked by rapid fluctuations and elevated energy release—that differ from isolated events of similar magnitude. These observations suggest that waveform analysis, particularly through the lens of early envelope behavior, may offer indirect constraints on the state of stress of faults and their potential to host a larger rupture. This has direct implications for the ongoing debate on whether foreshocks reflect preparatory processes or stochastic clustering.

Although foreshocks are frequently observed before large earthquakes, they also occur prior to smaller events, making their predictive significance uncertain (E. E. Brodsky, 2011; de Arcangelis et al., 2016; Lippiello et al., 2012, 2017; Moutote et al., 2021; Ogata & Katsura, 2014; Petrillo & Lippiello, 2020, 2023; Seif et al., 2018; Shearer, 2012; Trugman & Ross, 2019; van den Ende & Ampuero, 2020). Two main models have been proposed. The cascade model (Fukao & Furumoto, 1985; Helmstetter & Sornette, 2003; Marsan & Enescu, 2012) views foreshocks as typical earthquakes that can occasionally trigger a larger rupture through stress transfer, without reflecting any special physical state. In contrast, the pre-slip model (Dodge et al., 1996; Ellsworth & Berzosa, 1995) suggests that foreshocks mark the onset of a preparatory process, where localized aseismic slip gradually loads adjacent fault patches until dynamic rupture occurs. Support for this model includes geodetic observations of slow slip between foreshock and mainshock (Ito et al., 2013; A. Kato et al., 2012; E. E. Brodsky & Lay, 2014b), and seismicity changes such as a decreasing Gutenberg-Richter  $b$ -value prior to large events—opposite to the increase typically seen after mainshocks (Gulia & Wiemer, 2019; Gulia et al., 2018). Although the interpretation of  $b$ -value trends remains debated (DeSalvio & Rudolph, 2021), this pattern has been documented in multiple foreshock–mainshock sequences (Chan et al., 2024). For further context, see recent reviews (Martínez-Garzón & Poli, 2024; Peng & Lei, 2025).

In this study, we introduce a novel approach to foreshock analysis by identifying anomalous patterns in waveform envelopes. We show that these anomalies, quantified by our newly developed  $Q$  index, systematically appear in foreshocks preceding large earthquakes. Our results provide insight into the physical processes governing foreshock sequences and contribute to the broader discussion on the seismic signals that may precede major ruptures.

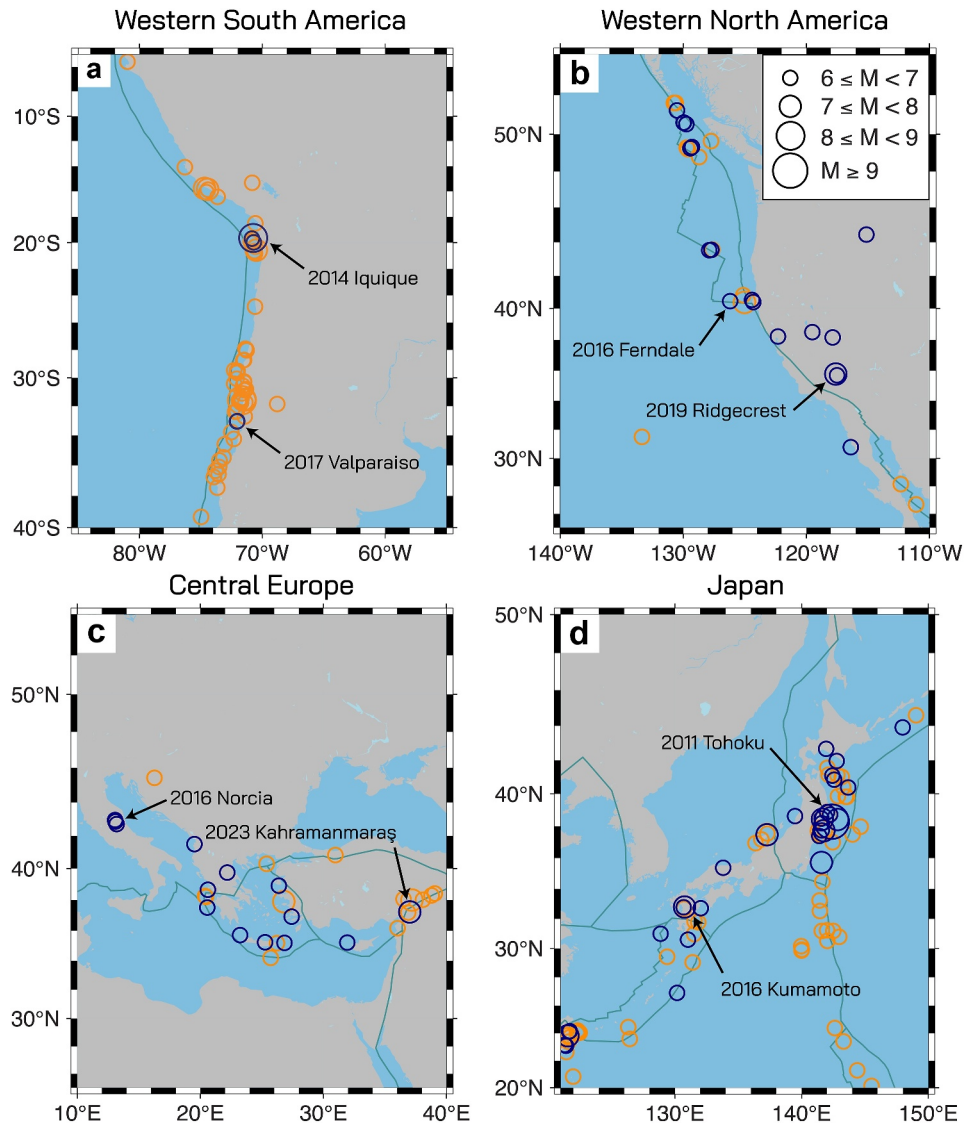


**Figure 1.** Overview of  $M_w 6+$  earthquakes analyzed in this study. (a) Western South America, (b) Western North America, (c) Central Europe, and (d) East Asia. Orange circles indicate all  $M_w 6+$  events from the USGS catalog (2011–2024), while blue circles highlight the subset selected for waveform analysis. Additional fore-mainshock pairs since 2011, including those outside the primary study regions, are also included. Circle size scales with event magnitude. Plate boundaries are shown for reference.

## 2. Methods and Results

The central quantity in our analysis is the envelope function  $\mu(t)$ , defined as the logarithm of the envelope of the ground velocity (Kanasewich, 1981) (see Supporting Information S1) (Figure 2). Prior to an earthquake,  $\mu(t)$  fluctuates around a background level  $\mu_B$ , before rising sharply and reaching a maximum value  $\mu_M$  at time  $t_M$ , corresponding to the perceived magnitude at the recording station (Lippiello et al., 2016).

The post-mainshock evolution of  $\mu(t)$  is strongly influenced by aftershock activity (Lippiello et al., 2016; Lippiello, Cirillo, et al., 2019; Lippiello, Petrillo, Godano, et al., 2019; Peng et al., 2007; Sawazaki & Enescu, 2014). Figures 2a and 2b illustrate two contrasting cases: the 27 December 2019  $M_w 6.1$  Kissamos earthquake, which was followed by no significant aftershocks ( $\mu \leq \mu_B$ ), and the 20 July 2017  $M_w 6.6$  Kos earthquake, which exhibited multiple large-amplitude secondary peaks consistent with elevated aftershock productivity in the hours following the mainshock. Following its peak at  $t = t_M$ , the envelope function  $\mu(t)$  of the  $M_w 6.1$  Kissamos earthquake decays rapidly and stabilizes at the background level,  $\mu(t) \approx \mu_B$ , consistent with an absence of aftershock activity. In

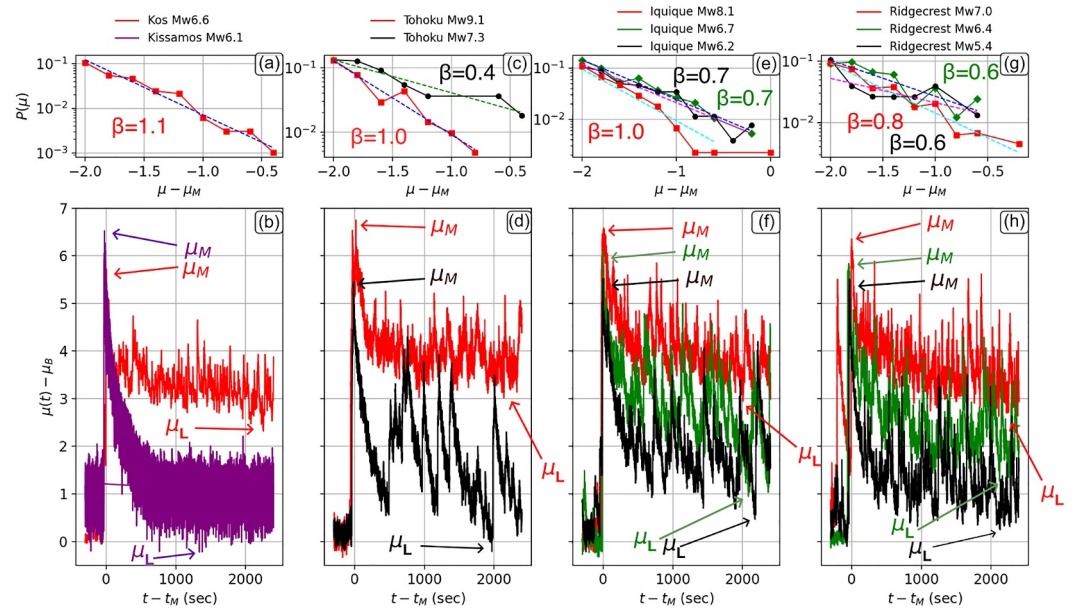


**Figure 2.** Envelope function  $\mu(t)$  (lower panels) and peak distribution  $P(\mu)$  (upper panels). Dashed lines in panels (a–d) represent the exponential distribution  $P(\mu) \propto 10^{-\beta\mu}$ , with colors indicating best-fit  $\beta$  values. Panels (a) and (b) show two extreme aftershock scenarios: the 2018  $M_w$ 6.6 Kos earthquake (red, many aftershocks) and the 2019  $M_w$ 6.1 Kissamos earthquake (violet, no aftershocks for  $\mu > \mu_B$ ). Panels (c) and (d) depict the 2011 Tohoku sequence: the  $M_w$ 9.1 mainshock (red) and  $M_w$ 7.3 foreshock (black). Panels (e–f) and (g–h) show results for Iquique and Ridgecrest events, respectively.

contrast, for the  $M_w$ 6.6 Kos earthquake,  $\mu(t)$  does not decay directly to  $\mu_B$ , but instead remains elevated, fluctuating around a plateau level  $\mu_L \gg \mu_B$ . The background level is only recovered after several weeks (Lippiello et al., 2016; Lippiello, Petrillo, Godano, et al., 2019; Shearer & Senobari, 2025), well beyond the time window shown in Figure 2b. This plateau is a hallmark of intense aftershock activity (Lippiello et al., 2016): when an aftershock occurs at time  $t_1 > t_M$  with perceived magnitude  $\mu_1$ , the envelope remains elevated at  $\mu(t_1) = \mu_1$ , preventing an immediate return to  $\mu_B$ .

If a second aftershock with perceived magnitude  $\mu_2$  occurs at  $t_2 > t_1$ , the envelope rises again, reaching  $\mu(t_2) = \mu_2 > \mu_B$ . When aftershock productivity is high, the interval  $(t_2 - t_1)$  between successive aftershocks is short, preventing  $\mu(t)$  from dropping below the plateau level  $\mu_L \approx \min(\mu_1, \mu_2) > \mu_B$ . Numerical simulations (Lippiello et al., 2016) show that the number of aftershocks increases exponentially with  $\mu_L - \mu_B$ . More specifically, the expected number of aftershocks ( $\mu_i > \mu_M - 2$ ) following a mainshock of perceived magnitude  $\mu_M$  scales as  $n_{aft} \propto 10^{-\delta\mu}$ , where  $\delta\mu = (\mu_M - \mu_B) - 2(\mu_L - \mu_B)$ . A detailed estimate of aftershock probability from  $\mu(t)$  in the first minutes after  $t_M$  is provided in Lippiello, Petrillo, Godano, et al. (2019).

The envelope function after the  $M_w$ 9.1 Tohoku earthquake of 11 March 2011 (Figures 2c and 2d) exhibits the expected high plateau level  $\mu_L$ , reflecting intense aftershock activity. However, the behavior observed after the  $M_w$ 7.3 Tohoku foreshock (Figures 2c and 2d) is strikingly different. In the first 8 minutes,  $\mu(t)$  returns to values close to  $\mu_B$ , resembling the no-aftershock pattern seen in the  $M_w$ 6.1 Kissamos earthquake (Figure 2b). Unlike Kissamos, however, the Tohoku foreshock envelope undergoes abrupt rises and falls, forming an anomalous sawtooth pattern. Large peaks in  $\mu(t)$  correspond to significant foreshocks ( $\mu_i \approx \mu_B + 4$ ), whereas valleys with  $\mu(t) \approx \mu_B$  indicate periods with very few  $\mu_i > \mu_B$  events. This contradicts the Gutenberg–Richter law, which predicts thousands of events with  $\mu_i \approx \mu_B + 1$  for every event with  $\mu_i \approx \mu_B + 4$ . It also challenges the cascade model, which interprets fore-mainshock sequences as typical triggering processes. In this model, a mainshock is simply an earthquake that happens to be larger than its triggering event, that is, the foreshock. The occurrence of an aftershock larger than the triggering event is expected in periods of intense aftershock activity (Fukao & Furumoto, 1985; Helmstetter & Sornette, 2003; Spassiani et al., 2024). Consequently, the cascade model would predict an envelope function  $\mu(t)$  with a high plateau level  $\mu_L$ , reflecting a large aftershock count  $n_{aft}$ . However, the observed envelope profile (black curve in Figure 2d) instead reveals the opposite trend: the Tohoku foreshock exhibited a limited ability to trigger small aftershocks.

This contrast between foreshock and mainshock envelope behavior is consistently observed across different seismic stations located at varying azimuths and distances from the rupture (see Text S6 in Supporting Information S1). Examining the evolution of  $\mu(t)$  in other foreshock-mainshock sequences reveals a similar pattern. Figures 2f and 2h show the envelope function  $\mu(t)$  for the  $M_w$ 8.1 1 April 2014 Iquique earthquake and the  $M_w$ 7.1 6 July 2019 Ridgecrest earthquake, respectively. In both cases, the mainshock envelope exhibits a high plateau level,  $\mu \gg \mu_B$ , indicating intense aftershock activity. In contrast, the envelopes of their large foreshocks (Figures 2f and 2h) display the sawtooth pattern similar to that observed in the Tohoku foreshock. This recurring behavior across multiple earthquake sequences suggests that waveform envelopes may provide valuable insights into foreshock-mainshock dynamics.

## 2.1. Quantifying Foreshock Waveform Anomalies

To systematically evaluate the observed differences in the envelope function (Figure 2), we introduce a quantitative measure to assess the degree of anomaly in a given envelope. This measure enables us to distinguish between normal envelopes and those exhibiting a sawtooth-like pattern.

Under normal conditions, the peak distribution  $P(\mu)$  follows the Ishimoto-Iida law (Ishimoto & Iida, 1939), expressed as  $P(\mu_i) \sim 10^{-\beta\mu_i}$ , where  $\beta$  is approximately equal to the  $b$ -value of the Gutenberg-Richter law. Consequently, the probability of an earthquake with perceived magnitude  $\mu_M$  being followed by a larger event is proportional to  $10^{-\beta\mu}$ . However, in foreshock sequences, the number of observed earthquakes  $n_{obs}$  with high peak values ( $\mu_i > \mu_M - 2$ ) may significantly exceed the number of expected aftershocks estimated assuming that no further fault segments or systems become unstable as a consequence of the stress redistribution promoted by previous events  $n_{aft} \propto 10^{-\delta\mu}$ , which is estimated from the plateau level  $\mu_L$ . The ratio  $n_{obs}/n_{aft}$  should therefore exhibit anomalously large values during foreshock sequences. To quantify this, we define the anomaly index  $Q = (n_{obs}/n_{aft}) 10^{-\beta\mu_M}$  (see Text S2 in Supporting Information S1). The number of observed peaks,  $n_{obs}$ , is determined following the method by Peng et al. (2007) for  $\mu(t)$  in the first 45 min after the mainshock. Given that the number of significant peaks is typically small and well separated, a manual count ensures accurate identification of local maxima  $\mu_i$  exceeding the threshold  $\mu_i > \mu_M - 2$ .

To test this approach systematically, we analyze all  $M_w$ 6+ earthquakes worldwide since 2011, including additional fore-mainshock pairs from Western South America (Figure 1a), and all  $M_w$ 6+ events since 2015 in the three primary study regions shown in Figures 1b–1d. These are defined as an  $M_w$ 6+ event followed within 10 days and 50 km by an event of equal or greater magnitude, with additional quality criteria applied (Text S3 in Supporting Information S1). The complete list is provided in Text S5 in Supporting Information S1. Most events are located in regions with dense seismic networks, such as inland Japan, Central Europe, and Western North America, with additional cases from Central and South America. The data set includes 68  $M$ 6+ earthquakes. Of these, 11 were followed within 10 days by a larger earthquake at an epicentral distance of less than 50 km, classifying them as foreshocks. The full selection and classification procedure is described in detail in the Text S5 in Supporting Information S1 together with the seismic network and station chosen for the download. We initially assume  $\beta = 1$  in the definition of  $Q$  and classify earthquakes as *anomalous* if  $Q \geq Q_{th}$  and *regular* if  $Q < Q_{th}$ . The value of  $Q$  for all 68 events is provided in Text S5 in Supporting Information S1 and plotted in Figure 3a. Setting  $Q_{th} = 0.18$ , we find that 10 of the 11 foreshocks in the data set are correctly classified as anomalous ( $Q \geq Q_{th}$ ), while 53 of the 57 non-foreshock events are correctly classified as normal ( $Q < Q_{th}$ ). Thus, only one foreshock is a missed alarm, and seven of 64 normal events are false alarms. Figure 3 demonstrates that anomalous earthquakes are strongly associated with foreshocks.

To further validate this classification, we use a receiver operating characteristic (ROC) diagram. This approach allows for a variable threshold  $Q_{th}$  instead of a fixed one, enabling us to assess the accuracy of our classification. Specifically, we apply a binary decision rule, triggering an alarm when  $Q \geq Q'$ , and compute the true positive rate (TPR), defined as the fraction of detected foreshocks among all foreshocks in the data set. We also evaluate the false alarm rate (FAR), defined as the fraction of non-foreshock events incorrectly classified as foreshocks. By varying  $Q'$ , we obtain the ROC curve (Figure 3b), which shows points near the ideal prediction scenario (TPR = 1, FAR = 0) and significantly above the random prediction line (TPR = FAR). The null hypothesis of random classification is rejected with confidence level  $cl > 99\%$ , supporting the conclusion that anomalous earthquakes are statistically associated with foreshocks. Further differences between foreshocks and mainshocks emerge in the peak distribution  $P(\mu)$  (Text S4 in Supporting Information S1). For instance, in the Tohoku

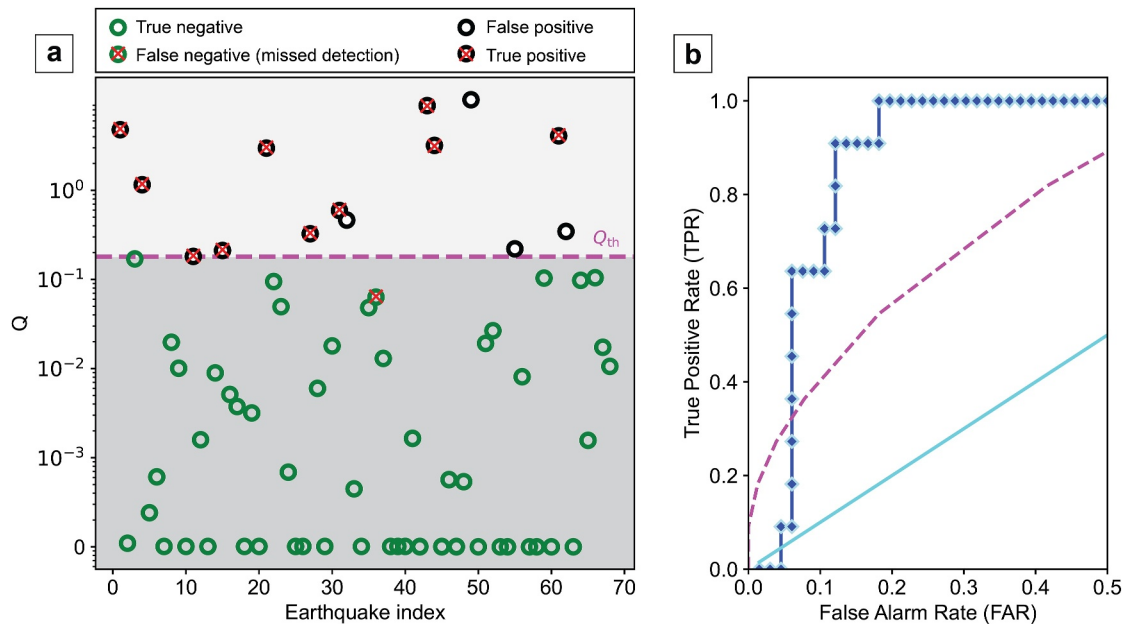


**Figure 3.** (a)  $Q$  values for all analyzed earthquakes, plotted in chronological order. Events classified as anomalous ( $Q \geq Q_{th}$ ) are shown in black, while normal events ( $Q < Q_{th}$ ) are in green. The threshold  $Q_{th} = 0.18$  is marked by a dashed magenta line. Foreshocks, defined as earthquakes followed within 10 days by a larger event within 50 km, are indicated by red cross. (b) Receiver operating characteristic curve showing the true positive rate (TPR, blue diamonds) versus the false alarm rate for the  $Q$ -value method with  $\beta = 1$ . The cyan diagonal represents the null hypothesis (random classification), while points above the dashed magenta line reject it with >99% confidence. Additional details and results for  $\beta$  extracted from the peak distribution are provided in Text S5 and S8 in Supporting Information S1.

sequence, the  $\beta$ -value after the  $M_w 7.3$  foreshock ( $\beta = 0.4 \pm 0.1$ ) is significantly lower than after the  $M_w 9.1$  mainshock ( $\beta = 1.0 \pm 0.1$ ). This change in  $\beta$  is consistent with the  $b$ -value decrease observed by Gulia and Wiemer (2019) and is observed in other foreshock-mainshock sequences (Figure 2, upper panels).

Incorporating  $\beta$  from  $P(\mu)$  into the  $Q$  index, rather than assuming  $\beta = 1$  (as in Figure 3), could improve foreshock identification. However, unlike parameters such as  $\mu_L$ ,  $\mu_B$ , and  $\mu_M$ , which can be estimated within the first hour of the envelope function, determining  $\beta$  requires a longer temporal window and a sufficient number of peaks for a reliable fit using the Ishimoto-Iida law. When  $\beta$  is available, the  $Q$  index improves foreshock discrimination, correctly identifying all foreshocks as anomalous with only three false alarms (Text S8 in Supporting Information S1). The  $\beta$  values used in this study were estimated using the maximum likelihood method introduced by Aki (1965). Although more advanced estimators, such as the b-more-positive method (Lippiello & Petrillo, 2024), can yield more accurate values under certain conditions the aim of our study is not to optimize  $\beta$  estimation per se. Rather, we use  $\beta$  to explore how the  $Q$  index relates to the statistical characteristics of the envelope.

### 3. Discussion and Conclusions

We have shown that foreshock waveforms often exhibit a distinct sawtooth-shaped envelope, characterized by multiple energy bursts and a prolonged decay. This pattern differentiates them from isolated events of similar magnitude and suggests a fundamentally different underlying process. A physical interpretation, consistent with the pre-slip model, is illustrated in Figure 4.

Prior to a large rupture, the impending rupture zone can be envisioned as a locked segment composed of multiple rate-weakening fault patches embedded within rate-strengthening surroundings (Figure 4a). Due to frictional heterogeneity, some patches approach failure earlier than others and may rupture. Two outcomes may follow. If adjacent regions are not critically stressed, the rupture remains confined, producing an isolated foreshock. In this case, the envelope function  $\mu(t)$  decays after the main peak, reflecting local relaxation without broader fault activation. Alternatively, if the stress perturbation engages neighboring patches that are also near failure, a cascade may ensue, culminating in a large rupture that propagates across the fault system (Figure 4c). In this scenario, the resulting waveform exhibits a characteristic sawtooth-like envelope, reflecting successive bursts of seismic energy from spatially distributed failure. If the rupture continues to propagate and activates a large portion

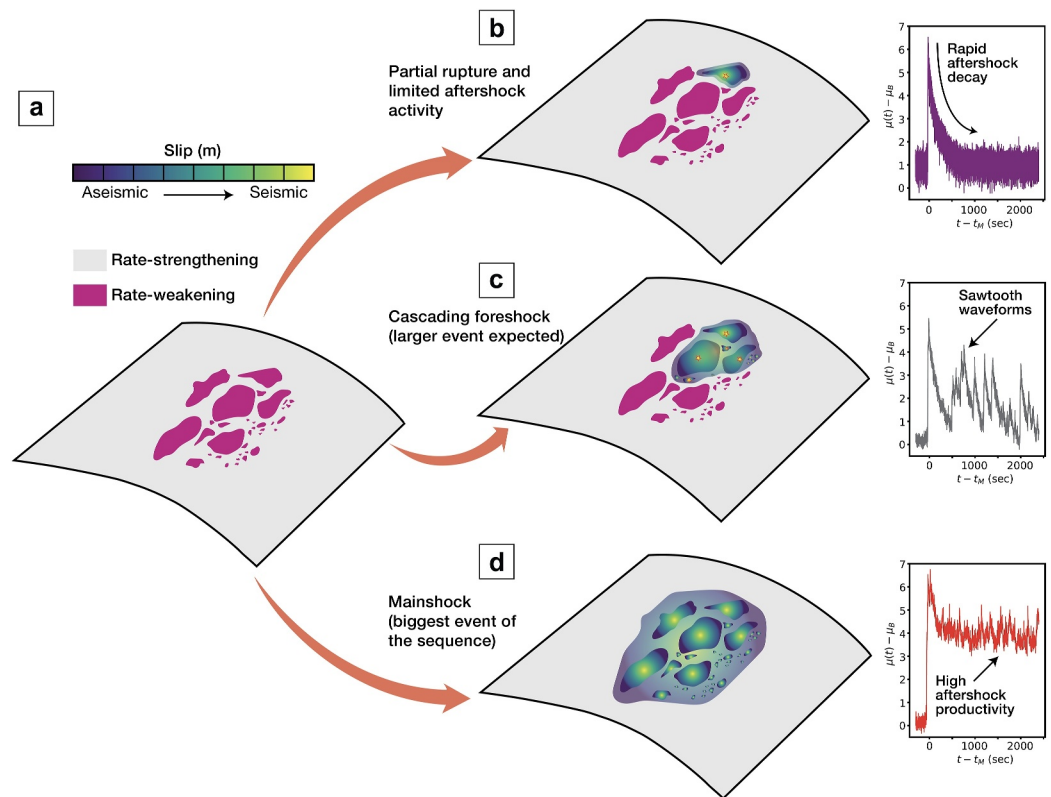


**Figure 4.** Conceptual model linking fault structure, rupture evolution, and the waveform envelope  $\mu(t)$ . (a) Schematic view of a fault region prior to failure, consisting of multiple rate-weakening patches (magenta) embedded within a rate-strengthening matrix (gray). (b) Partial rupture scenario: slip on a single unstable patch does not trigger adjacent patches. Stress is redistributed within the surrounding strengthening region, producing limited aftershock activity and a rapidly decaying envelope  $\mu(t)$  (right, violet). (c) Cascading foreshock: seismic slip on one patch engages neighboring critically stressed patches, resulting in a sequence of interacting failures. The resulting envelope shows a sawtooth-shaped pattern (right, gray), reflecting successive energy bursts from spatially distributed slip. (d) Mainshock scenario: rupture propagates through much of the locked zone, generating high aftershock productivity and a saturated envelope signal (right, red). In this case, the dense sequence of secondary events masks earlier sawtooth features, and  $\mu(t)$  remains at a high plateau.

of the fault, it evolves into the mainshock of the sequence (Figure 4d). In this case, the envelope is dominated by high-amplitude fluctuations resulting from intense aftershock activity. The dense sequence of secondary events rapidly fills the signal, masking any sawtooth-like features that might have preceded the rupture. Thus, while moderate foreshocks may exhibit a distinctive waveform fingerprint, these signatures become increasingly difficult to resolve as the system transitions toward full rupture and seismic saturation.

Our results suggest that as the fault approaches failure, the envelope function  $\mu(t)$  evolves into a sequence of discrete bursts separated by intervals where  $\mu(t) \simeq \mu_B$ . This pattern reflects the activation of isolated unstable patches within a locked region. The closer the fault is to global failure, the greater the number of critically stressed patches, and the more pronounced the sawtooth structure becomes. Following the mainshock, the redistribution of stress alters the spatial pattern of seismicity. Aftershocks tend to occur along the boundaries of the previously locked region, producing a sustained high plateau in  $\mu(t)$  (Figure 4d). Based on these dynamics, we identify three characteristic envelope behaviors: (a) A single sharp peak in  $\mu(t)$  followed by a rapid return to background levels ( $\mu \simeq \mu_B$ ) indicates localized slip within a locked fault that remains far from global failure. (b) A sustained high plateau ( $\mu_L \gg \mu_B$ ) is consistent with intense aftershock activity following a mainshock, suggesting that no larger event is imminent in the near future. (c) A sawtooth-shaped envelope with multiple energy bursts separated by quiet intervals reflects a foreshock occurring within a fault region nearing global failure, where several unstable patches are interacting.

This framework accounts for the observed envelope of the 2011  $M_w$ 7.3 Tohoku foreshock, as well as the 2014  $M_w$ 6.2 Iquique foreshock, both of which show pronounced sawtooth patterns (black curves in Figures 2d–2f). These events likely ruptured within the interior of the locked region, where the interaction of multiple unstable patches generated distinct bursts of seismic energy. In contrast, foreshocks that occur near the boundary of the locked region show a different behavior. In these cases, stress is partly transferred outward, triggering normal aftershock sequences. This scenario is exemplified by the 2014  $M_w$ 6.7 Iquique foreshock (Figure 2f), where  $\mu(t)$  decays to a low but nonzero plateau, indicating modest aftershock activity. At the same time, large isolated peaks reflect additional seismic bursts likely associated with foreshock dynamics.

A similar mixed pattern is observed in the 2019 Ridgecrest sequence. The  $M_w$ 6.4 foreshock, located on a secondary fault adjacent to the eventual rupture zone, generated both a weak aftershock sequence and large-amplitude bursts linked to foreshock activity on the main fault. This results in a low but nonzero  $\mu_L - \mu_B$  value, superimposed with sporadic peaks (green curve, Figure 2h). Notably, a  $M_w$ 5.4 foreshock occurred just 16 hr before the mainshock, within 2 km of its epicenter. Its envelope strongly resembles that of the  $M_w$ 7.3 Tohoku foreshock, suggesting a common underlying mechanism (black curve, Figure 2h).

Our findings demonstrate that foreshock sequences can be distinguished from typical aftershock sequences by analyzing ground velocity envelopes. Foreshocks preceding large earthquakes exhibit anomalous sawtooth-shaped waveforms, unlike the plateau-like patterns observed in aftershocks. These oscillations between high and low envelope values indicate the presence of multiple rate-weakening patches approaching failure.

We introduced the quantitative index  $Q$ , based on waveform anomalies, to assess the likelihood that an earthquake is a foreshock. Applied to a global data set of  $M6+$  events, the method successfully identified 10 foreshocks that preceded larger earthquakes within 10 days. The  $Q$  index is advantageous due to its straightforward formulation in terms of  $\mu_B$ ,  $\mu_L$ , and  $n_{obs}$ , which can be estimated within minutes of the main envelope peak (see Text S2 in Supporting Information S1). This approach addresses limitations in prior methods, such as the one proposed by Gulia and Wiemer (2019), which relies on earthquake-specific adjustments to define a reference  $b$ -value, potentially introducing bias (E. Brodsky, 2019; Marzocchi et al., 2019). In contrast, the  $Q$  index is universally defined and largely unaffected by aftershock detection biases (de Arcangelis et al., 2018).

While the method is robust and operationally simple, several factors that may influence  $Q$  remain to be systematically explored. These include sensitivity to the frequency band used to compute the envelope, variations in station geometry and epicentral distance, source depth, and the finite extent of large ruptures. Although our results show consistency across stations and parameter choices, a more detailed analysis of these effects would strengthen the generality of the approach. We hope this work provides a foundation for future efforts to better constrain the physical and observational limits of waveform-based foreshock identification.

To advance short-term seismic hazard assessment, waveform-based methods like the  $Q$  index should be integrated with independent indicators of fault stress evolution, such as spatial and temporal variations in the  $b$ -value (Gulia & Wiemer, 2019). Large foreshocks often induce Coulomb stress changes that correlate with  $b$ -value anomalies (Nanjo, 2020), offering insight into the evolving state of the fault. For example, a sustained decrease in  $b$ -value was observed over several years prior to the 2011 Tohoku earthquake (Nanjo et al., 2012; Tormann et al., 2015), whereas an increase was documented near the mainshock hypocenter in the 2016 Kumamoto sequence (Nanjo & Yoshida, 2017). While the  $b$ -value captures longer-term stress accumulation, the  $Q$  index provides a near-instantaneous measure of waveform anomalies linked to cascading failure. Combined, these approaches offer complementary perspectives on fault loading and rupture potential. We suggest that future operational strategies for earthquake forecasting should explore multi-parameter frameworks that integrate waveform features with seismicity-based stress indicators.

### Conflict of Interest

The authors declare no conflicts of interest relevant to this study.

### Data Availability Statement

The event information can be downloaded on the website <https://earthquake.usgs.gov/earthquakes/search/>, information about seismic stations and waveforms can be downloaded at <https://ds.iris.edu/gmap/>. For Japan data,

the waveform can be downloaded at <https://www.hinet.bosai.go.jp> For the last link, after completing the registration process, set a username and password, please proceed to the “Continuous Waveform Data Download” section. The code used to compute the envelope function is available at: <https://doi.org/10.5281/zenodo.15460925> (Petrillo, 2025) and <https://github.com/statmechcode/envelopefore/>.

### Acknowledgments

This study, as well as the contributions of G.P. and L.D.Z., was supported by the Earth Observatory of Singapore (EOS) and the Singapore Ministry of Education Tier 3b project “Investigating Volcano and Earthquake Science and Technology (InVEST)” (MOE-MOET32021-0002). E.L. acknowledges support from the MIUR PRIN 2022 PNRR (Grant P202247YKL), and C.G. acknowledges support from the MIUR PRIN 2022 PNRR (Grant P20222B5P9).

### References

- Aki, K. (1965). Maximum likelihood estimate of  $b$  in the formula  $\log n = a - bm$  and its confidence limits. *Earthquake Research Institute, The University of Tokyo*, 43, 237–239.
- Aki, K. (1967). Scaling law of seismic spectrum. *Journal of Geophysical Research*, 72(4), 1217–1231. <https://doi.org/10.1029/jz072i004p01217>
- Avouac, J.-P. (2015). From geodetic imaging of seismic and aseismic fault slip to dynamic modeling of the seismic cycle. *Annual Review of Earth and Planetary Sciences*, 43(1), 233–271. <https://doi.org/10.1146/annurev-earth-060614-105302>
- Beaucé, E., Poli, P., Waldhauser, F., Holtzman, B., & Scholz, C. (2023). Enhanced tidal sensitivity of seismicity before the 2019 magnitude 7.1 ridgecrest, California earthquake. *Geophysical Research Letters*, 50(14), e2023GL104375. <https://doi.org/10.1029/2023GL104375>
- Behr, W. M., & Bürgmann, R. (2021). What’s down there? The structures, materials and environment of deep-seated slow slip and tremor. *Philosophical Transactions of the Royal Society A: Mathematical, Physical and Engineering Sciences*, 379(2193), 20200218. <https://doi.org/10.1098/rsta.2020.0218>
- Bletery, Q., & Nocquet, J.-M. (2020). Slip bursts during coalescence of slow slip events in cascadia. *Nature Communications*, 11(1), 2159. <https://doi.org/10.1038/s41467-020-15494-4>
- Bletery, Q., & Nocquet, J.-M. (2023). The precursory phase of large earthquakes. *Science*, 381(6655), 297–301. <https://doi.org/10.1126/science.adg2565>
- Bletery, Q., & Nocquet, J.-M. (2025). Do large earthquakes start with a precursory phase of slow slip? *Seismica*, 3(2). <https://doi.org/10.26443/seismica.v3i2.1383>
- Bradley, K., & Hubbard, J. A. (2023). Earthquake precursors? Not so fast. *Earthquake Insights*. <https://doi.org/10.62481/310cc439>
- Bradley, K., & Hubbard, J. A. (2024). Precursory slip before large earthquakes—Signal or noise? *Earthquake insights*. <https://doi.org/10.62481/0ff960fa>
- Brodsky, E. (2019). Predicting if the worst earthquake has passed. *Nature*, 574(7777), 185–186. <https://doi.org/10.1038/d41586-019-02972-z>
- Brodsky, E. E. (2011). The spatial density of foreshocks. *Geophysical Research Letters*, 38(10), L10305. <https://doi.org/10.1029/2011GL047253>
- Brodsky, E. E., & Lay, T. (2014a). Recognizing foreshocks from the 1 April 2014 Chile earthquake. *Science*, 344(6185), 700–702. <https://doi.org/10.1126/science.1255202>
- Brodsky, E. E., & Lay, T. (2014b). Recognizing foreshocks from the 1 April 2014 Chile earthquake. *Science*, 344(6185), 700–702. <https://doi.org/10.1126/science.1255202>
- Chan, C.-H., Kao, J.-C., & Chen, D.-Y. (2024). Spatial-temporal variations of b-values prior to medium-to-large earthquakes in Taiwan and the feasibility of real-time precursor monitoring. *Earth Planets and Space*, 76(1), 119. <https://doi.org/10.1186/s40623-024-02065-w>
- Cicerone, R. D., Ebel, J. E., & Britton, J. (2009). A systematic compilation of earthquake precursors. *Tectonophysics*, 476(3–4), 371–396. <https://doi.org/10.1016/j.tecto.2009.06.008>
- Cohen, S. C. (1999). Numerical models of crustal deformation in seismic zones. *Advances in Geophysics*, 41, 133–231. [https://doi.org/10.1016/s0065-2687\(08\)60027-8](https://doi.org/10.1016/s0065-2687(08)60027-8)
- de Arcangelis, L., Godano, C., Grasso, J. R., & Lippiello, E. (2016). Statistical physics approach to earthquake occurrence and forecasting. *Physics Reports*, 628, 1–91. <https://doi.org/10.1016/j.physrep.2016.03.002>
- de Arcangelis, L., Godano, C., & Lippiello, E. (2018). The overlap of aftershock coda-waves and short-term post seismic forecasting. *Journal of Geophysical Research: Solid Earth*, 123(7), 5661–5674. <https://doi.org/10.1029/2018JB015518>
- DeSalvo, N. D., & Rudolph, M. L. (2021). A retrospective analysis of b-value changes preceding strong earthquakes. *Seismological Research Letters*, 93(1), 364–375. <https://doi.org/10.1785/0220210149>
- Dieterich, J. H., & Kilgore, B. (1996). Implications of fault constitutive properties for earthquake prediction. *Proceedings of the National Academy of Sciences*, 93(9), 3787–3794. <https://doi.org/10.1073/pnas.93.9.3787>
- Dodge, D. A., Beroza, G. C., & Ellsworth, W. L. (1996). Detailed observations of California foreshock sequences: Implications for the earthquake initiation process. *Journal of Geophysical Research*, 101(B10), 22371–22392. <https://doi.org/10.1029/96JB02269>
- Ellsworth, W. L., & Beroza, G. C. (1995). Seismic evidence for an earthquake nucleation phase. *Science*, 268(5212), 851–855. <https://doi.org/10.1126/science.268.5212.851>
- Felzer, K. R., Abercrombie, R. E., & Ekstrom, G. (2004). A common origin for aftershocks, foreshocks, and multiplets. *Bulletin of the Seismological Society of America*, 94(1), 88–98. <https://doi.org/10.1785/0120030069>
- Fineberg, J., & Marder, M. (1999). Instability in dynamic fracture. *Physics Reports*, 313(1–2), 1–108. [https://doi.org/10.1016/s0370-1573\(98\)00085-4](https://doi.org/10.1016/s0370-1573(98)00085-4)
- Fukao, Y., & Furumoto, M. (1985). Hierarchy in earthquake size distribution. *Physics of the Earth and Planetary Interiors*, 37(2), 149–168. [https://doi.org/10.1016/0031-9201\(85\)90048-2](https://doi.org/10.1016/0031-9201(85)90048-2)
- Gomberg, J., the Cascadia 2007, & Group, B. W. (2010). Slow-slip phenomena in Cascadia from 2007 and beyond: A review. *GSA Bulletin*, 122(7–8), 963–978. <https://doi.org/10.1130/B30287.1>
- Gulia, L., Rinaldi, A. P., Tormann, T., Vannucci, G., Enescu, B., & Wiemer, S. (2018). The effect of a mainshock on the size distribution of the aftershocks. *Geophysical Research Letters*, 45(24), 13277–13287. <https://doi.org/10.1029/2018GL080619>
- Gulia, L., & Wiemer, S. (2019). Real-time discrimination of earthquake foreshocks and aftershocks. *Nature*, 574(7777), 193–199. <https://doi.org/10.1038/s41586-019-1606-4>
- Helmstetter, A., & Sornette, D. (2003). Foreshocks explained by cascades of triggered seismicity. *Journal of Geophysical Research*, 108(B10), 2457. <https://doi.org/10.1029/2003JB002409>
- Hulbert, C., Rouet-Leduc, B., Johnson, P. A., Ren, C. X., Rivière, J., Bolton, D. C., & Marone, C. (2019). Similarity of fast and slow earthquakes illuminated by machine learning. *Nature Geoscience*, 12(1), 69–74. <https://doi.org/10.1038/s41561-018-0272-8>
- Ishimoto, M., & Iida, K. (1939). Observations sur les seismes enregistres parle microsismographe construit dernièrement. *Bulletin of the Earthquake Research Institute*, 17, 443–478.
- Ito, Y., Hino, R., Kido, M., Fujimoto, H., Osada, Y., Inazu, D., et al. (2013). Episodic slow slip events in the Japan subduction zone before the 2011 Tohoku-Oki earthquake. *Tectonophysics*, 600, 14–26. <https://doi.org/10.1016/j.tecto.2012.08.022>

- Kanasewich, E. (1981). *Time sequence analysis in geophysics* (3rd ed.). University of Alberta.
- Kaneko, Y., Nielsen, S. B., & Carpenter, B. M. (2016). The onset of laboratory earthquakes explained by nucleating rupture on a rate-and-state fault. *Journal of Geophysical Research: Solid Earth*, *121*(8), 6071–6091. <https://doi.org/10.1002/2016JB013143>
- Kato, A., & Ben-Zion, Y. (2021). The generation of large earthquakes. *Nature Reviews Earth & Environment*, *2*(1), 26–39. <https://doi.org/10.1038/s43017-020-00108-w>
- Kato, A., Obara, K., Igarashi, T., Tsuruoka, H., Nakagawa, S., & Hirata, N. (2012). Propagation of slow slip leading up to the 2011 Mw 9.0 Tohoku-Oki earthquake. *Science*, *335*(6069), 705–708. <https://doi.org/10.1126/science.1215141>
- Kato, N. (2020). Complexity in the earthquake cycle increases with the number of interacting patches. *Pure and Applied Geophysics*, *177*(10), 4657–4676. <https://doi.org/10.1007/s00024-020-02555-4>
- Kazemian, J., Tiampo, K., Klein, W., & Dominguez, R. (2015). Foreshock and aftershocks in simple earthquake models. *Physical Review Letters*, *114*(8), 088501. <https://doi.org/10.1103/physrevlett.114.088501>
- Kumagai, H., Pulido, N., Fukuyama, E., & Aoi, S. (2012). Strong localized asperity of the 2011 Tohoku-oki earthquake, Japan. *Earth Planets and Space*, *64*(7), 649–654. <https://doi.org/10.5047/eps.2012.01.004>
- Lay, T., & Kanamori, H. (1981). An asperity model of large earthquake sequences. Earthquake prediction: An. *International Review*, *4*, 579–592.
- Lee, J., Tsai, V. C., Hirth, G., Chatterjee, A., & Trugman, D. T. (2024). Fault-network geometry influences earthquake frictional behaviour. *Nature*, *631*(8019), 106–110. <https://doi.org/10.1038/s41586-024-07518-6>
- Lei, X. (2003). How do asperities fracture? An experimental study of unbroken asperities. *Earth and Planetary Science Letters*, *213*(3–4), 347–359. [https://doi.org/10.1016/s0012-821x\(03\)00328-5](https://doi.org/10.1016/s0012-821x(03)00328-5)
- Lippiello, E., Cirillo, A., Godano, C., Papadimitriou, E., & Karakostas, V. (2019). Post seismic catalog incompleteness and aftershock forecasting. *Geosciences*, *9*(8), 355. <https://doi.org/10.3390/geosciences9080355>
- Lippiello, E., Cirillo, A., Godano, G., Papadimitriou, E., & Karakostas, V. (2016). Real-time forecast of aftershocks from a single seismic station signal. *Geophysical Research Letters*, *43*(12), 6252–6258. <https://doi.org/10.1002/2016GL069748>
- Lippiello, E., Giacco, F., Marzocchi, W., Godano, C., & Arcangelis, L. D. (2017). Statistical features of foreshocks in instrumental and ETAS catalogs. *Pure and Applied Geophysics*, *174*(4), 1–19. <https://doi.org/10.1007/s00024-017-1502-5>
- Lippiello, E., Marzocchi, W., de Arcangelis, L., & Godano, C. (2012). Spatial organization of foreshocks as a tool to forecast large earthquakes. *Scientific Reports*, *2*, 1–6. <https://doi.org/10.1038/srep00846>
- Lippiello, E., Petrillo, C., Godano, C., Tramelli, A., Papadimitriou, E., & Karakostas, V. (2019). Forecasting of the first hour aftershocks by means of the perceived magnitude. *Nature Communications*, *10*(1), 2953. <https://doi.org/10.1038/s41467-019-10763-3>
- Lippiello, E., & Petrillo, G. (2024). b-more-incomplete and b-more-positive: Insights on a robust estimator of magnitude distribution. *Journal of Geophysical Research: Solid Earth*, *129*(2), e2023JB027849. <https://doi.org/10.1029/2023JB027849>
- Lippiello, E., Petrillo, G., Landes, F., & Rosso, A. (2019). Fault heterogeneity and the connection between aftershocks and afterslip. *Bulletin of the Seismological Society of America*, *109*(3), 1156–1163. <https://doi.org/10.1785/0120180244>
- Lippiello, E., Petrillo, G., Landes, F., & Rosso, A. (2021). The genesis of aftershocks in spring slider models. In *Statistical methods and modeling of seismogenesis* (pp. 131–151). John Wiley & Sons, Ltd. <https://doi.org/10.1002/9781119825050.ch5>
- Marsan, D., & Enescu, B. (2012). Modeling the foreshock sequence prior to the 2011,  $M_w$ 9.0 Tohoku, Japan, earthquake. *Journal of Geophysical Research*, *117*(B6), 3837. <https://doi.org/10.1029/2011JB009039>
- Martínez-Garzón, P., & Poli, P. (2024). Cascade and pre-slip models oversimplify the complexity of earthquake preparation in nature. *Communications Earth & Environment*, *5*(1), 120. <https://doi.org/10.1038/s43247-024-01285-y>
- Marzocchi, W., Spassiani, I., Stallone, A., & Taroni, M. (2019). How to be fooled searching for significant variations of the b-value. *Geophysical Journal International*, *220*(3), 1845–1856. <https://doi.org/10.1093/gji/ggz541>
- McLaskey, G. C. (2019). Earthquake initiation from laboratory observations and implications for foreshocks. *Journal of Geophysical Research: Solid Earth*, *124*(12), 12882–12904. <https://doi.org/10.1029/2019jb018363>
- Mignan, A. (2014). The debate on the prognostic value of earthquake foreshocks: A meta-analysis. *Scientific Reports*, *4*(1), 4099. <https://doi.org/10.1038/srep04099>
- Moutote, L., Marsan, D., Lengliné, O., & Duputel, Z. (2021). Rare occurrences of non-cascading foreshock activity in southern California. *Geophysical Research Letters*, *48*(7), e2020GL091757. <https://doi.org/10.1029/2020GL091757>
- Nanjo, K. Z. (2020). Were changes in stress state responsible for the 2019 ridgecrest, California, earthquakes? *Nature Communications*, *11*(1), 3082. <https://doi.org/10.1038/s41467-020-16867-5>
- Nanjo, K. Z., Hirata, N., Obara, K., & Kasahara, K. (2012). Decade-scale decrease in b value prior to the M9-class 2011 Tohoku and 2004 Sumatra quakes. *Geophysical Research Letters*, *39*(20), L20304. <https://doi.org/10.1029/2012GL052997>
- Nanjo, K. Z., & Yoshida, A. (2017). Anomalous decrease in relatively large shocks and increase in the p and b values preceding the April 16, 2016, M7.3 earthquake in Kumamoto, Japan. *Earth Planets and Space*, *69*(1), 13. <https://doi.org/10.1186/s40623-017-0598-2>
- Obara, K., & Kato, A. (2016). Connecting slow earthquakes to huge earthquakes. *Science*, *353*(6296), 253–257. <https://doi.org/10.1126/science.aaf1512>
- Ogata, Y., & Katsura, K. (2014). Comparing foreshock characteristics and foreshock forecasting in observed and simulated earthquake catalogs. *Journal of Geophysical Research: Solid Earth*, *119*(11), 8457–8477. <https://doi.org/10.1002/2014JB011250>
- Okada, Y. (1985). Surface deformation due to shear and tensile faults in a half-space. *Bulletin of the Seismological Society of America*, *75*(4), 1135–1154. <https://doi.org/10.1785/bssa0750041135>
- Passelègue, F. X., Latour, S., Schubnel, A., Nielsen, S., Bhat, H. S., & Madariaga, R. (2017). Influence of fault strength on precursory processes during laboratory earthquakes. In *Fault zone dynamic processes* (pp. 229–242). American Geophysical Union (AGU). <https://doi.org/10.1002/9781119156895.ch12>
- Pelletier, J. D. (2000). Spring-block models of seismicity: Review and analysis of a structurally heterogeneous model coupled to a viscous asthenosphere. In *Geocomplexity and the physics of earthquakes* (pp. 27–42). American Geophysical Union (AGU). <https://doi.org/10.1029/GM120p0027>
- Peng, Z., & Lei, X. (2025). Physical mechanisms of earthquake nucleation and foreshocks: Cascade triggering, aseismic slip, or fluid flows? *Earthquake Research Advances*, *5*(2), 100349. <https://doi.org/10.1016/j.eqrea.2024.100349>
- Peng, Z., Vidale, J. E., Ishii, M., & Helmstetter, A. (2007). Seismicity rate immediately before and after main shock rupture from high-frequency waveforms in Japan. *Journal of Geophysical Research*, *112*(B3), B03306. <https://doi.org/10.1029/2006JB004386>
- Petrillo, G. (2025). statmechcode/envelopefore: V1.0.1 [Software]. *Zenodo*. <https://doi.org/10.5281/zenodo.15460925>
- Petrillo, G., Landes, F., Lippiello, E., & Rosso, A. (2020). The influence of the brittle-ductile transition zone on aftershock and foreshock occurrence. *Nature Communications*, *11*(1), 3010. <https://doi.org/10.1038/s41467-020-16811-7>

- Petrillo, G., & Lippiello, E. (2020). Testing of the foreshock hypothesis within an epidemic like description of seismicity. *Geophysical Journal International*, 225(2), 1236–1257. <https://doi.org/10.1093/gji/ggaa611>
- Petrillo, G., & Lippiello, E. (2023). Incorporating foreshocks in an epidemic-like description of seismic occurrence in Italy. *Applied Sciences*, 13(8), 4891. <https://doi.org/10.3390/app13084891>
- Pritchard, M. E., Allen, R. M., Becker, T. W., Behn, M. D., Brodsky, E. E., Bürgmann, R., et al. (2020). New opportunities to study earthquake precursors. *Seismological Society of America*, 91(5), 2444–2447. <https://doi.org/10.1785/0220200089>
- Reches, Z., & Fineberg, J. (2023). Earthquakes as dynamic fracture phenomena. *Journal of Geophysical Research: Solid Earth*, 128(3), e2022JB026295. <https://doi.org/10.1029/2022jb026295>
- Rubin, A. M., & Ampuero, J.-P. (2005). Earthquake nucleation on (aging) rate and state faults. *Journal of Geophysical Research*, 110(B11), 2161. <https://doi.org/10.1029/2005JB003686>
- Sato, T., & Hirasawa, T. (1973). Body wave spectra from propagating shear cracks. *Journal of Physics of the Earth*, 21(4), 415–431. <https://doi.org/10.4294/jpe1952.21.415>
- Sawazaki, K., & Enescu, B. (2014). Imaging the high-frequency energy radiation process of a main shock and its early aftershock sequence: The case of the 2008 Iwate—Miyagi Nairiku earthquake, Japan. *Journal of Geophysical Research: Solid Earth*, 119(6), 4729–4746. <https://doi.org/10.1002/2013JB010539>
- Scholz, C., Sykes, L., & Aggarwal, Y. (1973). Earthquake prediction: A physical basis. *Science*, 181(4102), 803–810. <https://doi.org/10.1126/science.181.4102.803>
- Schwartz, S. Y., & Rokosky, J. M. (2007). Slow slip events and seismic tremor at circum-pacific subduction zones. *Reviews of Geophysics*, 45(3), RG3004. <https://doi.org/10.1029/2006rg000208>
- Seif, S., Zechar, J. D., Mignan, A., Nandan, S., & Wiemer, S. (2018). Foreshocks and their potential deviation from general seismicity. *Bulletin of the Seismological Society of America*, 109(1), 1–18. <https://doi.org/10.1785/0120170188>
- Seif, S., Zechar, J. D., Mignan, A., Nandan, S., & Wiemer, S. (2019). Foreshocks and their potential deviation from general seismicity. *Bulletin of the Seismological Society of America*, 109(1), 1–18. <https://doi.org/10.1785/0120170188>
- Shearer, P. M. (2012). Self-similar earthquake triggering, bath's law, and foreshock/aftershock magnitudes: Simulations, theory, and results for southern California. *Journal of Geophysical Research*, 117(B6), B06310. <https://doi.org/10.1029/2011jb008957>
- Shearer, P. M., & Senobari, N. S. (2025). Continuous aftershock hum for over ten days following the 2019 Ridgecrest, California, earthquakes observed with borehole seismometers.
- Spasiani, I., Petrillo, G., & Zhuang, J. (2024). Distribution related to all samples and extreme events in the ETAS cluster. *Seismological Research Letters*, 95(6), 3234–3242. <https://doi.org/10.1785/0220230324>
- Tormann, T., Enescu, B., Woessner, J., & Wiemer, S. (2015). Randomness of megathrust earthquakes implied by rapid stress recovery after the Japan earthquake. *Nature Geoscience*, 8(2), 152–158. <https://doi.org/10.1038/ngeo2343>
- Trugman, D. T., & Ross, Z. E. (2019). Pervasive foreshock activity across southern California. *Geophysical Research Letters*, 46(15), 8772–8781. <https://doi.org/10.1029/2019GL083725>
- van den Ende, M. P. A., & Ampuero, J.-P. (2020). On the statistical significance of foreshock sequences in southern California. *Geophysical Research Letters*, 47(3), e2019GL086224. <https://doi.org/10.1029/2019GL086224>
- Wyss, M. (1991). Evaluation of proposed earthquake precursors. *Eos, Transactions American Geophysical Union*, 72(38), 411. <https://doi.org/10.1029/90eo10300>
- Zaccagnino, D., Vallianatos, F., Michas, G., Telesca, L., & Doglioni, C. (2024). Are foreshocks fore-shocks? *Journal of Geophysical Research: Solid Earth*, 129(2), e2023JB027337. <https://doi.org/10.1029/2023jb027337>